and their almost identity in the three complexes indicate that a comparable but not strong apical interaction by solvent molecules occurs to these copper(II) centers. The $g_{\parallel}$ value increases significantly on replacement of the thiolate sulfur (CuN_2SS^* core of $[Cu(pyt\text{-}N,S\text{-}im)]^{2+}$) by an oxygen donor ($CuN_2OS^*$ core of $[Cu(sal\text{-}N,S\text{-}im)]^{+}$) in the copper coordination sphere, in spite of a reduction in the formal positive charge of the complex.[66] Moreover, the $g_{\parallel}$ and $A_{\parallel}$ values found here for CuN_2SS^* compare well with the corresponding values reported for the CuN_2S_2 cores of the copper(II) complexes of II ($g_{\parallel} = 2.140$, $A_{\parallel} = 184 \times 10^{-4}$ cm^{-1}; formal charge of the complex 2+)[32] and of the ligands derived from the condensation of ethylenediamine and two molecules of thiosalicylaldehyde ($g_{\parallel} = 2.121$, $A_{\parallel} = 186 \times 10^{-4}$ cm^{-1}; formal charge of the complex 0)[8] or related thiocarbonyl compounds.[9] The decrease in $g_{\parallel}$ and increase in $A_{\parallel}$ values in this series of complexes is in accord with the established trends of covalency.[20,66]

In conclusion, the present investigation has shown that I can provide an useful source of thiolate ligands to form stable copper(II)–thiolate complexes and that, by proper choice of the residue to be conjugated with I, it is possible to obtain ligand systems with donor sets that mimic those found in the blue proteins. The metal complexes of pyt-N,S-im reported here are apparently the first systems containing a N_2SS^* ligand donor set. The spectroscopic properties of the copper(II) complex are substantially determined by the presence of the thiolate sulfur donor, while binding by the other donor atoms can only be inferred by appropriate substitution analogues. Although this pyt-N,S-im ligand cannot provide to the metal a low-symmetry environment such as that of the protein blue sites, it is known from model studies[31,67] that an increase in the size of the fused chelate rings can lead to a significant distortion of the metal geometry. Thus, it is expected that ligand homologues of pyt-N,S-im containing longer carbon chains between the donor atoms will give rise to copper(II) complexes that progressively approach the spectral behavior of the blue sites. The synthesis of such ligand systems is currently under way in this laboratory. Finally, while the attention is usually focused only on the spectral properties of copper(II) model systems, it is important to give parallel development to the characterization of the corresponding copper(I) systems, even though they generally exhibit poor spectral properties. We have shown in this and in previous studies[50,51c] that careful examination of the solution behavior of copper(I) complexes can give useful information about the groups involved in metal binding.

Acknowledgment. This work was supported by a grant from the Italian MPI. I thank the Italian CNR for instrumentation facilities, M. Bonfà for recording the NMR spectra, P. Russo for recording the MS spectra, and C. Pessina for assistance in the synthesis of 1-phenyl-3-formyl-2(1*H*)-pyridinethione.

Registry No. I, 61856-49-3; III, 91002-69-6; [IV][ClO_4] (M = Cu(I)), 91002-60-7; [IV][ClO_4]$_2$ (M = Cu(II)), 91002-62-9; [IV][ClO_4]$_2$ (M = Zn(II)), 91002-64-1; [V][ClO_4], 91002-66-3; [VI][ClO_4]$_2$, 91002-68-5; 4-{[(2-aminoethyl)thio]methyl}-5-methylimidazole, 38585-67-0.

(66) (a) Peisach, J.; Blumberg, W. E. *Arch. Biochem. Biophys.* **1974**, *165*, 691–708. (b) Addison, A. W. In ref 59, pp 109–128.

(67) (a) Martin, J. W. L.; Timmons, J. H.; Martell, A. E.; Rudolf, P.; Clearfield, A.; Willis, C. J. *J. Chem. Soc., Chem. Commun.* **1979**, 999–1000. (b) Martin, J. W. L.; Timmons, J. H.; Martell, A. E.; Willis, C. J. *Inorg. Chem.* **1980**, *19*, 2328–2331. (c) Timmons, J. H.; Rudolf, P.; Martell, A. E.; Martin, J. W. L.; Clearfield, A. *Ibid.* **1980**, *19*, 2331–2338.

Contribution from the Departments of Chemistry, The Chung-Cheng Institute of Technology, Taiwan, Republic of China, and The University of Mississippi, University, Mississippi 38677

Lower Valence Fluorides of Chromium. 1. The Hexagonal Bronze Type Phase Rb_xCrF_3

Y. S. HONG,[†] K. N. BAKER,[‡] R. F. WILLIAMSON,[‡] and W. O. J. BOO*[‡]

Received September 27, 1983

Samples of Rb_xCrF_3 having compositions $x = 0.18$, 0.20, 0.225, 0.25, 0.275, and 0.30 were prepared and studied. The hexagonal bronze-like system spans the range $x = 0.18$–0.29. An orthorhombic sublattice ($a \approx 12.7$ Å, $b \approx 7.4$ Å, and $c \approx 7.4$ Å) was identified in every sample. Modulated structures resulting from $^1/_2$-, $^2/_3$-, and $^3/_4$-filled Rb^+ sites have compositions $x = 0.167$, 0.222, and 0.250 and are designated $\alpha(0.167)$, $\alpha(0.222)$, and $\alpha(0.250)$, respectively. The $\alpha(0.167)$ unit cell has the same dimensions as the orthorhombic sublattice, but unlike the sublattice, which is primitive, the superstructure is body centered. The $\alpha(0.222)$ unit cell has the same a and b dimensions as the sublattice, but it is base centered with c(super) = $^3/_2c$(sub). The $\alpha(0.250)$ phase has a primitive unit cell with dimensions a(super) = $2a$(sub), b(super) = $3b$(sub), and c(super) = $2c$(sub). Cooperative Jahn–Teller ordering is associated with $\alpha(0.222)$ and $\alpha(0.250)$, indicating Cr^{2+}–Cr^{3+} ordering (electronic ordering) in those phases. In samples where $x = 0.20$, 0.225, 0.25, and 0.275, $|a|/(3^{1/2}|b|)$ (the distortion ratio) is 0.98, but this ratio approaches unity at the limiting compositions $x = 0.18$ and 0.29. An undistorted hexagonal bronze phase was also observed in samples where $x = 0.20$, 0.225, 0.25, and 0.275. Magnetic interactions in Rb_xCrF_3 are predominantly antiferromagnetic, but Cr^{2+}–Cr^{3+} nearest-neighbor interactions appear to be ferromagnetic. In samples where $x = 0.18$, 0.20, and 0.225, short-range ordering sets in near 125 K. Long-range ordering at all compositions occurs between 35 and 25 K.

Introduction

The fluoride systems A_xVF_3,[1] A_xCrF_3,[2] and A_xFeF_3[3] (where A = K, Rb, or Cs and $x \approx 0.20$–0.30) were originally reported to crystallize in the hexagonal tungsten bronze structure, space group $P6_3/mcm$.[4] The vanadium fluorides (A = K, Rb, Tl, or Cs) were carefully prepared and intensively characterized in our laboratory[5–9] by polarized microscopy, high-precision

[†] The Chung-Cheng Institute of Technology.
[‡] The University of Mississippi.

(1) Cros, C.; Feurer, R.; Pouchard, M.; Hagenmuller, P. *Mater. Res. Bull.* **1975**, *10*, 383.
(2) Dumora, D.; Ravez, J.; Hagenmuller, P. *J. Solid State Chem.* **1972**, *5*, 35.
(3) Tressaud, A.; DePape, R.; Portier, J.; Hagenmuller, P. *Bull. Soc. Chim. Fr.* **1970**, *10*, 3411.
(4) Magneli, A. *Acta Chem. Scand.* **1953**, *7*, 315.

0020-1669/84/1323-2787$01.50/0

X-ray powder diffraction, and low-temperature magnetic measurements. Rieck et al.[10,11] studied these same materials by transmission electron microscopy, employing electron diffraction and lattice-imaging technqiues.

Superlattice reflections on X-ray and electron diffraction photographs, as well as lattice images, confirmed ordering of A^+ ions in partially filled sites. Guinier–Hagg X-ray diffraction studies revealed unique superlattices for which A^+ sites are $^1/_2$, $^2/_3$, and $^3/_4$ filled. The hexagonal bronze structure consists of hexagonal layers stacked along the c axis, and three superstructures [designated $\alpha(0.167)$, $\alpha(0.222)$, and $\alpha(0.250)$] have repeating dimensions along the c axis of two, three, and four layers, respectively. The $\alpha(0.167)$ and $\alpha(0.222)$ phases were found in A_xVF_3 systems where A = K, Rb, or Tl, but the $\alpha(0.250)$ phase appeared only in the Rb and Tl systems. No evidence of A^+ ordering was observed in the Cs_xVF_3 compounds. Guinier–Hagg studies also revealed that symmetry in each of the A_xVF_3 systems is lower than hexagonal over their entire composition span. Cooperative Jahn–Teller ordering of the V^{3+} ion distorts the orthohexagonal unit cell such that $|a|/(3^{1/2}|b|)$ (the distortion ratio) is either greater than 1 or less than 1. In the K_xVF_3 system, the distortion ratio is 1.007 for values of x below 0.26 and is 0.992 for x above 0.26; in both Rb_xVF_3 and Tl_xVF_3, the distortion ratio is 1.005 below $x = 0.24$ and is 0.992 above $x = 0.24$; but in Cs_xVF_3, the ratio is approximately 0.997 at all compositions.

At low temperatures, magnetic properties of the A_xVF_3 compounds are composition dependent. The $\alpha(0.222)$ phase, for example, displays a spontaneous magnetic moment, but $\alpha(0.167)$ and $\alpha(0.250)$ do not. This feature, along with a proposed superstructure of A^+ ions in $\alpha(0.222)$, leads to the conclusion that V^{2+}–V^{3+} electronic ordering is also present in this phase.

Dumora et al.[2] reported neither superlattice structures nor distortions of the orthohexagonal unit cells in A_xCrF_3 compounds. Since V^{3+} (a weak Jahn–Teller ion) distorts the hexagonal bronze lattice, one would expect Cr^{2+} (a much stronger Jahn–teller ion) to do the same. Furthermore, the question remains: "Are superstructures unique to the A_xVF_3 system?" One curious effect was reported, however.[2] An anomaly in hexagonal lattice dimensions of Rb_xCrF_3 was observed near the composition $x = 0.25$. This feature, along with several unanswered questions, has motivated this in-depth study of the Rb_xCrF_3 system.

Experimental Section

Appropriate quantities of RbF, CrF_2, and CrF_3 were vacuum encapsulated inside 1.91-cm diameter by 3.18-cm length molybdenum containers by means of electron-beam welding techniques. The solid-state reaction was carried out at 850 °C for a period of 28 days inside a Hevi-duty Lindberg tube furnace. Products were analyzed optically by stereoscopic and polarized microscopy. Chemical analyses were performed by Galbraith Laboratories. Rubidium and chromium were determined by atomic absorption (±2%), and fluorine was estimated by difference. Samples were characterized by Guinier–Hagg X-ray techniques using Cu $K\alpha_1$, and Cr $K\alpha_1$ radiations. Magnetic measurements were made from 4.2 to 300 K between 0.14 and 10 kG with a Foner-type PAR vibrating-sample magnetometer equipped with a Janis liquid-helium Dewar and gallium arsenide temperature controller. Magnetic fields were measured with a F. W. Bell hall-probe gaussmeter, Model 8860. Magnetic data were corrected for core diamagnetism from ionic susceptibility tables by Mulay.[12]

Table I. Chemical Analysis of Rb_xCrF_3 Compounds

	%		formula	
element	calcd	found	exptl	theor
Rb	12.37	12.21	$Rb_{0.178}CrF_{3.03}$	$Rb_{0.18}CrF_3$
Cr	41.81	41.69		
F	45.83			
Rb	13.56	13.39	$Rb_{0.197}CrF_{2.99}$	$Rb_{0.20}CrF_3$
Cr	41.24	41.42		
F	45.20			
Rb	15.00	14.95	$Rb_{0.225}CrF_{3.02}$	$Rb_{0.225}CrF_3$
Cr	40.55	40.42		
F	44.45			
Rb	16.39	16.31	$Rb_{0.250}CrF_{3.03}$	$Rb_{0.25}CrF_3$
Cr	39.89	39.73		
F	43.72			
Rb	17.74	17.68	$Rb_{0.274}CrF_{2.99}$	$Rb_{0.275}CrF_3$
Cr	39.24	39.31		
F	43.02			

Table II. Orthorhombic Dimensions of the Sublattice, Distortion Ratios of the Pseudohexagonal (Orthorhombic) Phase, Modulated Structures Present, and Lattice Dimensions of the Undistorted Hexagonal Phase from Cr $K\alpha_1$ Data

sample	orthorhombic dimens ±0.1%	distortion ratio	modulated structure	hexagonal dimens ±0.2%
$Rb_{0.18}CrF_3$	12.68	0.991	α(0.167)	
	7.383		α(0.222)	
	7.411			
$Rb_{0.20}CrF_3$	12.66	0.982	α(0.167)	
	7.441		α(0.222)	7.34
	7.406			7.41
$Rb_{0.225}CrF_3$	12.62	0.978	α(0.167)	
	7.445		α(0.222)	7.35
	7.408			7.41
$Rb_{0.25}CrF_3$	12.61	0.980	α(0.167)	
	7.431		α(0.222)	7.35
	7.427		α(0.250)	7.42
$Rb_{0.275}CrF_3$	12.63	0.981	α(0.222)	
	7.431		α(0.250)	7.35
	7.431			7.43
$Rb_{0.30}CrF_3$	12.78	0.994	α(0.222)	
	7.423		α(0.250)	
	7.448			

Results

The transmitted color of the Rb_xCrF_3 hexagonal bronze-like system is amber, considerably more optically dense than CrF_3 (light green) or CrF_2 (greenish blue). The $Rb_{0.18}CrF_3$ sample contained a small amount of CrF_3 (rhombohedral), which was removed by Pasteur's method. The $Rb_{0.30}CrF_3$ sample contained $Rb_{0.45}CrF_3$ (orthorhombic), which was inseparable from the hexagonal phase. Chemical analyses of samples where $x = 0.18$–0.275 are shown in Table I. On the basis of chemical analyses and the amount to $Rb_{0.45}CrF_3$ present in the $Rb_{0.30}CrF_3$ sample (estimated from optical analysis and intensities of impurity lines on X-ray diffraction photographs), the composition of Rb_xCrF_3 is approximately $x = 0.18$–0.29.

X-ray Diffraction. Guinier–Hagg data for all of the Rb_xCrF_3 samples were fitted to orthorhombic sublattice unit cells of dimensions $a \approx 12.7$ Å, $b \approx 7.4$ Å, and $c \approx 7.4$ Å. Table II gives a summary of these dimensions and the distortion ratios. The values obtained by using Cu and Cr X-radiations agree within experimental error; hence, only the Cr results are given in Table II. Table III shows the low-angle Guinier–Hagg data for Rb_xCrF_3 in which Cr $K\alpha_1$ radiation

(5) Hong, Y. S.; Williamson, R. F.; Boo, W. O. J. *Inorg. Chem.* **1979**, *18*, 2123.
(6) Hong, Y. S.; Williamson, R. F.; Boo, W. O. J. *AIP Conf. Proc.* **1979**, *No. 53*, 388.
(7) Lee, Y. F.; Williamson, R. F.; and Boo, W. O. J. In "Solid State Chemistry: A Contemporary Overview"; Holt, S. L., Milstein, J. B., Robbins, M., Eds.; American Chemical Society: Washington, DC, 1980; Adv. Chem. Ser. No. 186, Chapter 17.
(8) Hong, Y. S.; Williamson, R. F.; Boo, W. O. J. *J. Chem. Educ.* **1980**, *57*, 583.
(9) Hong, Y. S.; Williamson, R. F; Boo, W. O. J. *Inorg. Chem.* **1981**, *20*, 403.
(10) Rieck, D.; Langley, R.; Eyring, L. *J. Solid State Chem.* **1982**, *45*, 259.
(11) Rieck, D.; Langley, R.; Eyring, L. *J. Solid State Chem.* **1983**, *48*, 100.
(12) Mulay, L. N. "Magnetic Susceptbility"; Interscience: New York, 1963; p 1782.

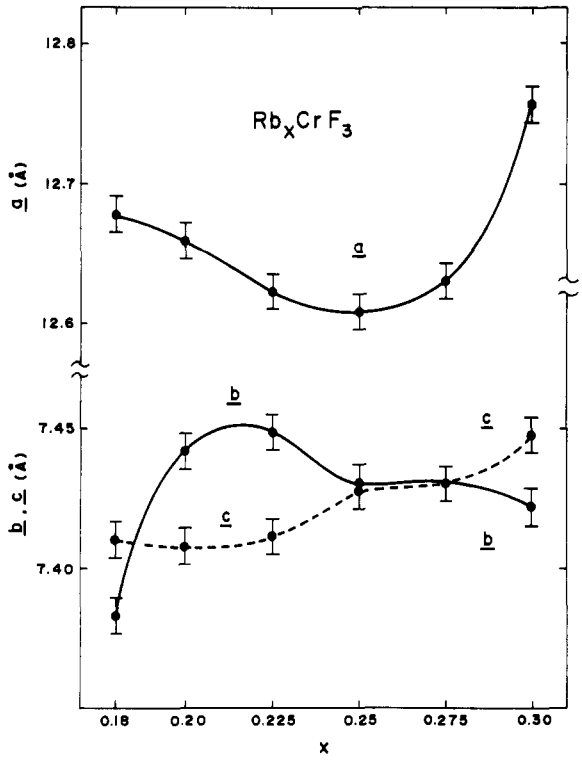

Figure 1. Orthorhombic lattice constants of Rb_xCrF_3 vs. x.

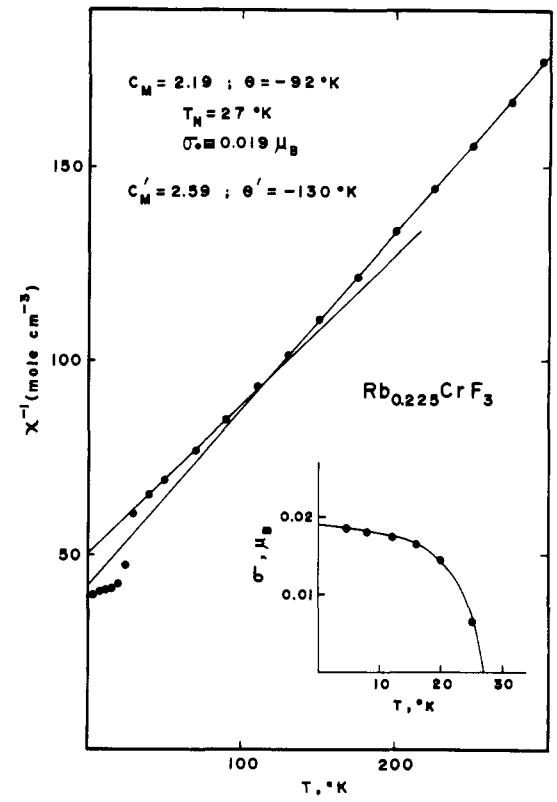

Figure 2. Inverse magnetic susceptibility vs. temperature for $Rb_{0.225}CrF_3$.

was used. The column in the far left gives hexagonal indicies from which the orthorhombic indicies are derived. These indicies correspond to the hexagonal bronze-like unit cell with $a \approx 7.4$ and $c \approx 7.4$ Å. The second column gives orthorhombic indicies of the sublattice and of the three superlattices. Both Table II and Table III use nominal values of x. The same three superstructures found in Rb_xVF_3[9] are present in the Rb_xCrF_3 system. Several reflections meeting the special conditions l = odd and $h + k + l = 2n$ have maximum intensities in the sample $Rb_{0.18}CrF_3$ but decrease in intensity as x increases. These reflections characterize a body-centered superlattice. Another set of reflections defining a superstructure where a(super) = a(sub), b(super) = b(sub), and c(super) = $^3/_2c$(sub) have maximum intensities in the sample where $x = 0.225$. All of these reflections obey the selection rule $h + k = 2n$, which characterizes a base-centered (C) superlattice. The third set of superlattice reflections with dimensions a(super) = $2a$(sub), b(super) = $3b$(sub), and c(super) = $2c$(sub) have maximum intensities for the sample where $x = 0.250$. In Table III, Miller indicies of the modulated structures that are optimum in samples $Rb_{0.18}CrF_3$, $Rb_{0.225}CrF_3$, and $Rb_{0.250}$ are indicated by single, double, and triple asterisks, respectively. Distortion ratios for all the samples are less than unity; however, the distortion of the orthohexagonal unit cell is large at compositions x = 0.20–0.275 but decreases at smaller and larger x. Furthermore, the values of b and c cross at two compositions and are essentially equal in samples of compositions $x = 0.25$ and 0.275. To dramatize these effects, a plot of a, b, and c vs. x is shown in Figure 1.

After calculated sublattice and superlattice values were fitted to the observed X-ray diffraction data of Rb_xCrF_3, a few lines in samples where $x = 0.20$, 0.225, 0.25, and 0.275 remained unidentified. Furthermore, some reflections identified as orthorhombic appeared broad or more intense than expected. In each sample these reflections were found to fit a simple hexagonal phase having dimensions $a \approx 7.35$ Å and $c \approx 7.42$ Å. From the relative intensities of these lines we estimate the amount of the hexagonal phase to be between 10 and 20% in each of the four samples. The dimensions of the hexagonal phases found in each sample are included in Table II. Table II also indicates which of the three superstructures are present in each sample.

Magnetic Measurements. A plot of the inverse magnetic susceptibility vs. temperature for $Rb_{0.225}CrF_3$ is shown in Figure 2. The usual paramagnetic region extends from high temperatures down to approximately 125 K. A second paramagnetic region extends from ~125 to 40 K. A small spontaneous moment that appears below 27 K is shown as an insert in Figure 2. The magnetic parameters are summarized in Table IV. Calculated values of C_M are obtained from

$$C_M = xC_{2+} + (1 - x)C_{3+}$$

For Cr^{3+} which is a spin-only system

$$C_{3+} = Ng_{3+}^2\mu_B^2(3/2)(3/2 + 1)/3k$$

and for Cr^{2+} in which the orbital moment is quenched below 300 K

$$C_{2+} = Ng_{2+}^2\mu_B^2(2)(2 + 1)/3k$$

where N is Avogadro's number, g_{2+} and g_{3+} are the Lande splitting factors for Cr^{2+} and Cr^{3+}, respectively, μ_B is the Bohr magneton, and k is the Boltzmann constant. Calculated values of C'_M are based on the assumption that each Cr^{2+} ion couples ferromagnetically with one Cr^{3+} ion. Thus

$$C'_M = xC_{2+,3+} + (1 - 2x)C_{3+}$$

where

$$C_{2+,3+} = Ng_{2+,3+}^2\mu_B^2(7/2)(7/2 + 1)/3k$$

If the values of g_{2+}, g_{3+}, and $g_{2+,3+}$ are assumed to be 2.00, $C_{3+} = 1.88$, $C_{2+} = 3.00$, and $C_{2+,3+} = 7.88$. Calculated values of C_M and C'_M shown in Table IV are for nominal values of x.

Discussion

One of the more dramatic aspects of the vanadium fluorides was their colors. The transmitted colors of VF_2 and VF_3 are

Table III. Guinier-Hagg X-ray Data for Orthorhombic Rb_xCrF_3 Cr $K\alpha_1$ Radiation ($\lambda = 2.289\,62$ Å)[a]

hexagonal (*hkil*)	orthorhombic (*hkl*)	*d*(obsd)/*I* *d*(calcd)					
		$Rb_{0.18}CrF_3$	$Rb_{0.20}CrF_3$	$Rb_{0.225}CrF_3$	$Rb_{0.25}CrF_3$	$Rb_{0.275}CrF_3$	$Rb_{0.30}CrF_3$
	001***				15.094/W^{-2} 14.855	15.169/W^{-3} 14.861	
	001**	11.235/W^{-2} 11.116	11.212/W^{-} 11.111	11.249/W^{-} 11.117	11.267/W^{-6} 11.141		11.275/W^{-5} 11.172
	002***				7.479/W^{-3} 7.427	7.479/W^{-4} 7.431	7.467/W^{-6} 7.448
	101*	6.424/S^{+} 6.398	6.395/M^{-} 6.393	6.453/W 6.391	6.439/W^{-4} 6.400		
$10\bar{1}0$	110	6.380/M^{-} 6.380	6.420/M^{-} 6.416	6.453/W 6.415	6.456/W^{-2} 6.402	6.444/W^{-2} 6.404	6.429/W^{-4} 6.419
	200	6.339	6.364/M^{-} 6.329	6.340/W^{-2} 6.311	6.367/W^{-3} 6.304	6.398/W^{-3} 6.315	6.392
	231*** 401***				5.919/W^{-2} 5.879 5.867/W^{-3} 5.803	5.922/W^{-2} 5.882 5.880/W^{-3} 5.812	
	002**	5.579/W^{-} 5.558	5.577/W 5.556	5.583/W^{+} 5.559	5.590/W^{+} 5.571	5.594/W^{-5} 5.573	5.584/W^{-3} 5.586
	111** 201**		5.577/W 5.555 5.515/W^{-4} 5.498	5.583/W^{+} 5.556 5.510/W^{-3} 5.488			
	011*	5.250/W 5.230	5.232/W^{-2} 5.250				
	322***				4.975/W^{-2} 4.980	4.969/W^{-4} 4.983	
	232*** 402***				4.860/W^{-2} 4.849 4.821/W^{-3} 4.806	4.870/W^{-3} 4.851 4.845/W^{-4} 4.812	4.878/W^{-3} 4.862 4.850/W^{-4} 4.851
	112** 202**	4.200/W^{-} 4.191 4.194/W^{-3} 4.179	4.205/W 4.200 4.183/W^{-} 4.175	4.213/W 4.201 4.185/W^{-} 4.171	4.208/W^{-4} 4.202 4.189/W^{-5} 4.174	4.218/W^{-6} 4.204 4.179	4.221/W^{-5} 4.214 4.204/W^{-6} 4.206
	211*	4.045/W 4.034	4.042/W^{-2} 4.041				
	342***				3.921/W 3.938	3.922/W^{-2} 3.940	
0002	002	3.713/S 3.705	3.710/S 3.704	3.716/S^{-} 3.706	3.720/M^{+} 3.714	3.726/M 3.715	3.730/W^{+} 3.724
$11\bar{2}0$	020 310	3.674/W^{-} 3.691 3.667	3.710/S 3.721 3.675/W^{-4} 3.671	3.725/W^{-} 3.724 3.669/W^{-4} 3.663	3.720/M^{+} 3.715 3.667/W^{-6} 3.658	3.726/M 3.715 3.675/W^{-5} 3.663	3.730/W^{+} 3.711 3.676/W^{-4} 3.696
	021** 311**		3.529 3.481/W^{-5} 3.485	3.536/W^{-6} 3.532 3.483/W^{-3} 3.479			
	062*** 632***				3.333/W^{-5} 3.323 3.282	3.334/W^{-6} 3.323 3.285	
$10\bar{1}2$	112 202	3.208/S^{+} 3.204 3.195/S^{+} 3.199	3.206/S^{+} 3.208 3.183/M 3.197	3.213/S^{+} 3.209 3.199/M 3.196	3.218/S^{+} 3.212 3.200/S 3.200	3.219/S^{+} 3.214 3.198/S^{-} 3.202	3.228/S 3.221 3.214/S^{+} 3.218
$20\bar{2}0$	220 400	3.195/S^{+} 3.190 3.176/M 3.169	3.206/S^{+} 3.208 3.159/M^{-} 3.165	3.213/S^{+} 3.208 3.157/S^{-} 3.155	3.212/S^{+} 3.201 3.168/S^{-} 3.152	3.219/S 3.202 3.176/M 3.158	3.214/S^{+} 3.210 3.196/S^{-} 3.196
	022** 312**		3.094/W^{-4} 3.092 3.061/W^{-4} 3.063	3.100/W^{-2} 3.094 3.062/W^{-2} 3.059	3.093/W^{-6} 3.091 3.058		
	222** 402**		2.778/W^{-4} 2.778 2.745/W^{-6} 2.750	2.780/W^{-2} 2.778 2.746/W^{-3} 2.744			

Table III (*Continued*)

hexagonal (*hkil*)	orthorhombic (*hkl*)	*d*(obsd)/*I* *d*(calcd)					
		$Rb_{0.18}CrF_3$	$Rb_{0.20}CrF_3$	$Rb_{0.225}CrF_3$	$Rb_{0.25}CrF_3$	$Rb_{0.275}CrF_3$	$Rb_{0.30}CrF_3$
		2.617/W⁻	2.626/W⁻	2.629/W	2.627/W⁺	2.629/W⁺	2.629/M
$11\bar{2}2$	022	2.615	2.625	2.627	2.627	2.627	2.629
		2.609/W	2.608/W⁺	2.606/W⁺	2.608/W	2.612/W⁻	2.621/W
	312	2.607	2.607	2.605	2.606	2.608	2.623

[a] **a*(super) = *a*(sub); *b*(super) = *b*(sub); *c*(super) = *c*(sub). ***a*(super) = *a*(sub); *b*(super) = *b*(sub); *c*(super) = 1.5*c*(sub). ****a*(super) = 2*a*(sub); *b*(super) = 3*b*(sub); *c*(super) = 2*c*(sub).

Table IV. Magnetic Constants of the Rb_xCrF_3 System

sample	C_M, cm³ deg mol⁻¹ obsd	calcd	C'_M, cm³ deg mol⁻¹ obsd	calcd	Θ, K	Θ′, K	T_N, K	σ, μ_B
$Rb_{0.18}CrF_3$	2.11	2.08	2.60	2.62	−100	−154	31	0.01
$Rb_{0.20}CrF_3$	2.19	2.10	2.64	2.70	−101	−146	29	0.01
$Rb_{0.225}CrF_3$	2.19	2.13	2.59	2.80	−92	−130	27	0.02
$Rb_{0.25}CrF_3$	2.27	2.16			−89		25	0.04
$Rb_{0.275}CrF_3$	2.26	2.19			−88		25	0.04
$Rb_{0.30}CrF_3$	2.24	2.21			−84		25	0.04

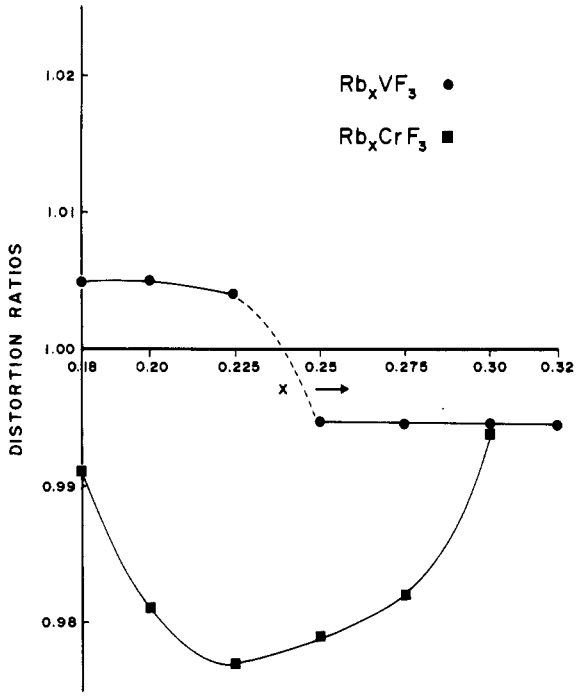

Figure 3. Distortion ratios for the orthohexagonal unit cells of Rb_xVF_3 and Rb_xCrF_3 vs. *x*.

blue and light green, respectively, but the mixed-valence compounds A_xVF_3 are brownish red and are almost opaque. By comparison, the transmitted colors of CrF_2 and CrF_3 are greenish blue and light green, respectively, but the color of the Rb_xCrF_3 phase is amber. The optical density of Rb_xCrF_3 is considerably greater than that of VF_2, VF_3, CrF_2, or CrF_3 but much less than that of the A_xVF_3 compounds.

The X-ray data of Rb_xCrF_3 have many interesting features. The sublattice and superlattice reflections, shown in Table III, are similar in identity and intensity to those published for Rb_xVF_3.[9] As in Rb_xVF_3, three superstructures were identified in Rb_xCrF_3. These are the same three superstructures, and X-ray intensities of each are optimum at the same compositions. One phenomenal differences between the two systems is in the distortions of the orthohexagonal unit cell. This is illustrated in Figure 3. In the vanadium system, the distortion ratio is approximately 1.005 for $x = 0.18$–0.24 and is 0.992 for $x = 0.24$–0.32. Although the orthohexagonal unit cell of

Table V. Comparison of Orthohexagonal Unit Cells

parameter	$Rb_{0.25}VF_3$[9]	$Rb_{0.25}CrF_3$	$Rb_{0.25}FeF_3$[3]
a, Å	12.835	12.608	12.75
b, Å	7.476	7.431	7.36
c, Å	7.569	7.427	7.53
distortion ratio	0.991	0.980	1.000
unit cell vol, Å³	726.3	695.8	706.6

Rb_xVF_3 displays one type of distortion below $x = 0.24$ and an opposite type above $x = 0.24$, the magnitude of the distortion is approximately constant over the entire composition range. The only correlation between the distortion ratio and the three phases is that the ratio is greater than unity when $\alpha(0.167)$ and $\alpha(0.222)$ are the prevalent phases and the ratio is less than unity when $\alpha(0.250)$ is prevalent. In the chromium system, the distortion of the orthohexagonal unit cell is always of the same kind [i.e. $|a|/(3^{1/2}|b|)$ is less than unity] but the magnitude of the distortion is composition dependent. In fact, the extent of distortion appears to depend upon the amount of $\alpha(0.222)$ and $\alpha(0.250)$ present. When the fraction of either or both of these phases diminishes, the distortion of the orthohexagonal unit cell is relaxed and the symmetry of the structure approaches true hexagonal. These effects can be qualitatively explained. In Rb_xVF_3, the Jahn–Teller ion is V^{3+}; its composition is $1 - x$; hence, it varies from 0.82 to 0.68. Since most of the vanadium sites are occupied by V^{3+}, it is not surprising that cooperative Jahn–Teller ordering exists at all compositions. In Rb_xCrF_3, the Jahn–Teller ion is Cr^{2+} but its composition is *x*; hence, it varies from 0.18 to 0.29. The fact that cooperative Jahn–Teller ordering is related to the $\alpha(0.222)$ and $\alpha(0.250)$ phases suggests that Cr^{2+}–Cr^{3+} ionic ordering (electronic ordering) also exists in these phases.

Table V shows lattice dimensions of the orthohexagonal unit cells of $Rb_{0.25}VF_3$,[9] $Rb_{0.25}CrF_3$, and $Rb_{0.25}FeF_3$.[3] For comparison, distortion ratios and unit cell volumes are also shown. Since the iron system is truly hexagonal, its orthohexagonal unit cell is undistorted; hence, its distortion ratio is 1.000. In addition to the smallest value for a distortion ratio (largest distortion), $Rb_{0.25}CrF_3$ has the smallest unit cell volume, and its values of *a* and *c* are significantly smaller than those of $Rb_{0.25}VF_3$ or $Rb_{0.25}FeF_3$. These effects are probably related to the lattice sites occupied by the Cr^{2+} ion and its orientation; however, a more quantitative evaluation would be highly speculative at this time. We presently have no plans to study this effect.

It is noteworthy that in the Rb_xCrF_3 system, the magnitudes of *b* and *c* are close at all compositions; in fact, they are identical within experimental error in samples where $x = 0.250$ and 0.275. (Relative intensities indicate Rb_xCrF_3 has a distorted Magneli hexagonal bronze structure, and even though *b* and *c* are equal, it should not be mistaken for a tetragonal system.) One would, therefore, expect boundary defects to be more numerous in the Rb_xCrF_3 system than in Rb_xVF_3. Rieck et al.[11] did in fact find evidence of "*bc*" or [010][001] boundaries in $K_{0.25}VF_3$. It is also quite likely that the presence of the Cr^{2+} ion, which has a shape significantly distorted from spherical, makes the parent CrF_3 lattice "elastic" and, con-

sequently, more inviting to defects of every kind.

Rieck et al.[10,11] reported the existence of a hexagonal phase in each of the Rb_xVF_3 samples. The hexagonal phase varies in composition and displays no apparent ionic ordering. We did not observe the hexagonal phase by X-ray diffraction because the distortion of the orthohexagonal unit cell is small in all of the A_xVF_3 materials and the true hexagonal reflections are obscured. In the Rb_xCrF_3 system, we actually observed hexagonal phases in the samples where $x = 0.20$, 0.225, 0.250, and 0.275. The electron microscopy studies (including electron diffraction as well as lattice imaging) also revealed the existence of orthorhombic symmetry in the Rb_xVF_3 samples. This was attributed to ordering of partially filled Rb^+ sites. This fits the description of the $\alpha(0.167)$ phase, which can be described as a hexagonal structure in which alternate rows of Rb^+ sites become either completely filled or completely empty along the *b* direction but rows of Rb^+ sites are occupied alternatively in both the *a* and *c* directions. This ordering destroys the hexagonal symmetry, of course. Rieck et al.[11] also observed ordering along the *c* axis in which the period was six layers deep. This corresponds quite well to our description of the $\alpha(0.222)$ phase in which ordering of partially occupied Rb^+ sites has a period of three layers along the *c* axis. Since the hexagonal bronze structure has a natural period of two layers, the true period of the $\alpha(0.222)$ phase should be 2×3 layers. No phase comparable to $\alpha(0.250)$ was observed by electron microscope techniques. There may be several reasons for this, the most obvious being that it is not a simple tunnel or layer structure; also, Rb^+ ordering may be altered by the intense electron beam. Rieck et al.[11] have demonstrated that defects in these phases are common, and they warn that defects may give rise to misinterpretation of X-ray and electron diffraction data. However, evidence that $\alpha(0.167)$, $\alpha(0.222)$, and $\alpha(0.250)$ are real phases is very good. First of all, the characteristic superlattice reflections are relatively intense. In sample $Rb_{0.18}CrF_3$, the reflections (designated by a single asterisk) 101 (S^+), 011 (W), and 211 (W), and several others at higher angles, lend support to the presence of a body centered orthorhombic superlattice. In sample $Rb_{0.225}CrF_3$, the reflections (with double asterisks) 001 (W^-), 002 (W^+), 111 (W^+), 201 (W^-), 112 (W), 202 (W^-), 021 (W^{-6}), 311 (W^{-3}), 022 (W^{-2}), 312 (W^{-2}), 222 (W^{-2}), and 402 (W^{-3}), and more at higher angles, support the presence of a layer structure with a repeating pattern, two layers of Rb^+ sites filled and one layer of Rb^+ sites empty, along the *c* axis. Finally, in sample $Rb_{0.250}CrF_3$, reflections (with triple asterisks) 001 (W^{-2}), 002 (W^{-3}), 231 (W^{-2}), 401 (W^{-3}, 322 (W^{-2}), 232 and 402 (W^{-2}), 342 (W), 062 and 632 (W^{-5}), and still more at higher angles, support the presence of a unique superlattice structure at this composition. Further arguments supporting the conclusion that these are true superlattices include the following: (1) $\alpha(0.167)$ corresponds to $^1/_2$ Rb^+ sites filled, $\alpha(0.222)$ has $^2/_3$ Rb^+ sites filled, and $\alpha(0.250)$ had $^3/_4$ Rb^+ sites filled. (2) The *c* dimension of these unit cells is dependent upon the Rb^+ site occupancy; that is, $\alpha(0.167)$, with $^1/_2$-filled sites, has *c* dimensions of two layers; in $\alpha(0.222)$, which is $^2/_3$ filled, *c* is three layers, and in $\alpha(0.250)$, which is $^3/_4$ filled, *c* is four layers deep. (3) The Rb_xCrF_3 system, in spite of differences in lattice dimensions, exhibits the same three superstructures found in the vanadium system. (4) In the Rb_xVF_3 system, a large spontaneous magnetic moment was linked to the $\alpha(0.222)$ phase. (5) In the Rb_xVF_3 system, cooperative Jahn–Teller ordering of V^{3+} distorts $\alpha(0.167)$ and $\alpha(0.222)$ one way but $\alpha(0.250)$ in the opposite way. (6) In the Rb_xCrF_3 system, cooperative Jahn–Teller ordering of Cr^{2+} exists only in the $\alpha(0.222)$ and $\alpha(0.250)$ phases. All of these experimental facts support our original conclusion that three distinct and ordered superstructures, each with a characteristic composition, exist within the framework of the parent lattice.

The general shape of the χ^{-1} vs. *T* plot shown in Figure 2 for $Rb_{0.225}CrF_3$ (aside from the fact that the linear region changes at ~120 K) is typical of ferrimagnetic materials. The large negative values of Θ shown in Table IV indicate that magnetic interactions are predominantly antiferromagnetic; however, some of the Cr^{2+}–Cr^{3+} nearest-neighbor interactions are expected to be ferromagnetic, which would have the effect of making Θ more positive. From Figure 2, the magnetic ordering temperature, T_N, is ~30 K. A more accurate value is obtained from plots of σ vs. *T*. Small spontaneous moments were observed at all compositions of Rb_xCrF_3, and values of T_N shown in Table IV are the temperatures at which σ approaches zero. The rule $T_N \approx |\Theta|$ for simple magnetic substances is not applicable as T_N is much smaller than Θ at all compositions. It is to be expected, however, that the value of T_N may be greatly reduced by constraints to magnetic ordering such as are inherent in the hexagonal bronze structure (simple magnetic constraints occur when nearest-neighboring metal ions have a common nearest neighbor and (1) interactions between all three are antiferromagnetic, (2) two of the three interactions are ferromagnetic and the third is antiferromagnetic, and/or (3) the phases of overlapping orbitals do not have the correct sign). The values of C_M from the high-temperature paramagnetic region confirm that the orbital moment in Cr^{2+} is totally quenched and that its moment is "spin only", as is that of Cr^{3+}.

The dependence of magnetic properties of Rb_xCrF_3 on structure and composition is very subtle. The magnitude of Θ and the value of T_N both decrease with increasing *x* as one would expect due to the increased concentration of Cr^{2+}. The spontaneous moment changes from approximately 0.01 to 0.04 μ_B as the superstructure changes from $\alpha(0.222)$ to $\alpha(0.250)$, respectively. Perhaps the most significant anomaly is the presence of two linear regions in χ^{-1} vs. *T* for samples where $x = 0.18$, 0.20, and 0.225 (those compositions where $\alpha(0.167)$ and $\alpha(0.222)$ are the predominant superstructure). The effect is not present at $x = 0.250$, 0.275, or 0.30 (those compositions where $\alpha(0.250)$ is the predominant superstructure). Changes of slope in χ^{-1} vs. *T* plots of first-row transition-metal fluorides are not uncommon. In VF_3 for example,[13] a first-order phase transition occurs near 120 K, which totally quenches a small orbital moment, giving rise to a second paramagnetic region. The orbital moment of Rb_xCrF_3 appears to be totally quenched at high temperatures; hence, one would not expect to observe this quenching effect at lower temperatures. In LiV_2F_6,[14] magnetic ordering occurs in steps; at ~100 K, ferromagnetic coupling occurs between nearest-neighboring V^{2+}–V^{3+} pairs, giving rise to a second linear region in a plot of χ^{-1} vs. *T*. This phenomenon was not expected in Rb_xCrF_3, but it is also not outside the realm of possibility. The ~180° magnetic interaction between Cr^{2+} and Cr^{3+} is predicted to be ferromagnetic from the rules of Goodenough[15] and Kanamori.[16] If one makes the assumption that each Cr^{2+} ion couples ferromagnetically with a single Cr^{3+} ion, the total spin of the complex would be $^7/_2$. The number of these dimers per mole would be *x*; then the second paramagnetic region would consist of *x* dimers with $S = ^7/_2$ and $1 - 2x$ Cr^{3+} ions with $S = ^3/_2$. For the compositions $x = 0.18$ and 0.20, the calculated and observed values of C'_M are nearly identical, but the fit is poor for $x = 0.225$. If we reexamine Table II, we see a hexagonal phase in samples where $x = 0.20$, 0.225, 0.250, and 0.275.

(13) Gossard, A. C.; Guggenheim, H. J.; Hsu, F. S. L.; Sherwood, R. C. *AIP Conf. Proc.* **1971**, *No. 5*, 302.
(14) Metzger, R. M.; Heimer, N. E.; Kuo, C. S.; Williamson, R. F.; Boo, W. O. J. *Inorg. Chem.* **1983**, *22*, 1060.
(15) Goodenough, J. B. "Magnetism and the Chemical Bond"; Interscience: New York, 1963; pp 165–185.
(16) Kanamori, J. *Phys. Chem. Solids* **1959**, *10*, 87.

Since the hexagonal phase is undistorted, one would not expect the formation of dimers to occur, thus reducing the effect in $Rb_{0.20}CrF_3$ and $Rb_{0.25}CrF_3$. The magnetic properties (except for C_M) may also be altered somewhat by structural defects that are expected to be even more common in Rb_xCrF_3 than in Rb_xVF_3.

Conclusions

The Rb_xCrF_3 system (x = 0.18–0.29) forms a Magneli hexagonal bronze-like lattice similar to the Rb_xVF_3 system. Ordering of partially filled Rb^+ sites forms superlattice structures in which sites are $^1/_2$, $^2/_3$, or $^3/_4$ filled. These superstructures are composition dependent and are optimum at compositions where x = 0.18, 0.225, and 0.25, respectively. Cooperative Jahn–Teller ordering of the Cr^{2+} ion is also composition dependent as it is associated with the superstructures α(0.222) and α(0.250). This leads to the conclusion that Cr^{2+}–Cr^{3+} electronic ordering exists in these two phases.

Acknowledgment. The authors gratefully acknowledge the National Science Foundation (Grant DMR 79-00313) for financial support and the University of Mississippi for cost sharing. Appreciation is expressed to the University of Mississippi Computer Center for providing data reduction time.

Registry No. Rubidium chromium fluoride, 37196-54-6.

Contribution from the Departments of Chemistry, Massachusetts Institute of Technology, Cambridge, Massachusetts 02139, and Columbia University, New York, New York 10027

Unusual Redox and Chemical Properties of a Sterically Constrained N_3Cu^{II} Center. Preparation, Structure, and Solution Studies of (Nitrato)(1,4,7-triazacyclododecane)copper(II) Nitrate

HARALD GAMPP, MICHAEL M. ROBERTS, and STEPHEN J. LIPPARD*

Received October 21, 1983

Dark blue crystals of $[Cu(TCD)(NO_3)](NO_3)$, TCD = 1,4,7-triazacyclododecane, form in the reaction of the free ligand with cupric nitrate in methanol. Linking of the terminal nitrogen atoms of the diethylenetriamine fragment of the TCD "minicycle" by a pentamethylene chain provides a steric constraint that substantially affects the properties of the $Cu(TCD)^{2+}$ cation. In particular, $Cu(TCD)^{2+}$ shows a quasi-reversible one-electron oxidation at −185 mV (vs. Fc/Fc^+), as compared with unconstrained $Cu(dien)^{2+}$, dien = 1,4,7-triazaheptane (diethylenetriamine), which exhibits an irreversible wave at an E_p of −450 mV by cyclic voltammetry under identical conditions ($LiClO_4$/acetonitrile solutions). Moreover, optical and electron spin resonance spectroscopic studies suggest that, whereas $Cu(dien)^{2+}$ binds one cyanide ligand strongly in its equatorial plane, $Cu(TCD)^{2+}$ coordinates two such cyanide ligands, with probable decoordination or substantial bond weakening of one of the nitrogen donors of the TCD group. Details of the geometric distortion produced by the TCD ligand were revealed in a single-crystal X-ray diffraction study of $[Cu(TCD)(NO_3)](NO_3)$, which crystallizes in the orthorhombic space group *Pnma*, a = 14.104 (2) Å, b = 8.882 (3) Å, c = 12.054 (1) Å, V = 1510 Å^3, and Z = 4. The structure is irregular and may be described as trigonal bipyramidal with axial positions occupied by one oxygen atom of a bidentate nitrate ligand and the central nitrogen atom of the TCD group. The major distortion found is the N–Cu–N′ angle of 138.6 (5)°, where N and N′ are related by a crystallographically required mirror plane of symmetry passing through the $[Cu(TCD)(NO_3)]^+$ cation. This angle is too small to span the trans basal positions of the usual tetragonal geometry for Cu(II), the structure adopted by $Cu(dien)^{2+}$ complexes, but not so small as to enforce facial type stereochemistry found with minicycles such as 1,4,7-triazacyclononane. The relevance of these results to copper(II) centers in metalloproteins is discussed.

Introduction

Recent efforts in our laboratory have focused on the chemistry of copper(II) in binucleating macrocycles, especially those having hexaaza donor functionalities such as A and A′.[1-3]

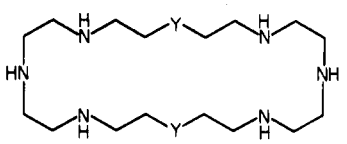

A, Y = O
A′, Y = CH_2

The synthetic routes[4] to these macrocycles give as a byproduct the triaza "minicycle" 1,4,7-triazacyclododecane (TCD). We

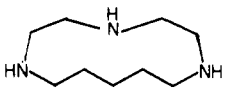

TCD

were interested to learn how the steric demands of this minicycle, achieved by connecting the terminal nitrogen atoms of the flexible 1,4,7-triazaheptane (diethylenetriamine, dien), would influence the coordination chemistry, spectroscopy, and redox properties of its copper(II) complex. Cupric complexes of cyclic triamines have been investigated by various authors;[5-16] relevant spectroscopic and stability data for these

* To whom correspondence should be addressed at the Massachusetts Institute of Technology.

(1) Martin, A. E.; Lippard, S. J. In "Copper Coordination Chemistry: Biochemical and Inorganic Perspectives"; Karlin, K. D., Zubieta, J. A., Eds.; Adenine Press: Guilderland, NY, 1983; p 395.
(2) (a) Coughlin, P. K.; Dewan, J. C.; Lippard, S. J.; Watanabe, E.-I.; Lehn, J.-M. *J. Am. Chem. Soc.* **1979**, *101*, 265. (b) Coughlin, P. K.; Martin, A. E.; Dewan, J. C.; Watanabe, E.-I.; Bulkowski, J. E.; Lehn, J.-M.; Lippard, S. J. *Inorg. Chem.* **1984**, *23*, 1004. (c) Coughlin, P. K.; Lippard, S. J. *J. Am. Chem. Soc.* **1981**, *103*, 3228. (d) Coughlin, P. K.; Lippard, S. J. *Ibid.* **1984**, *106*, 2328.
(3) (a) Coughlin, P. K.; Lippard, S. J.; Martin, A. E.; Bulkowski, J. E. *J. Am. Chem. Soc.* **1980**, *102*, 7616. (b) Martin, A. E.; Lippard, S. J. *Ibid.* **1984**, *106*, 2579.
(4) (a) Martin, A. E.; Bulkowski, J. E. *J. Org. Chem.* **1982**, *47*, 415. (b) Comarmond, J.; Plumeré, P.; Lehn, J.-M.; Agnus, Y.; Louis, R.; Weiss, R.; Kahn, O.; Morgenstern-Badarau, I. *J. Am. Chem. Soc.* **1982**, *104*, 6330.
(5) De Ronde, M.; Driscoll, D.; Yang, R.; Zompa, L. J. *Inorg. Nucl. Chem. Lett.* **1975**, *11*, 521.
(6) Yang, R.; Zompa, L. J. *Inorg. Chem.* **1976**, *15*, 1499.
(7) Zompa, L. J. *Inorg. Chem.* **1978**, *17*, 2531.
(8) Kodama, M.; Kimura, E. *J. Chem. Soc., Dalton Trans.* **1976**, 1720.
(9) Kodama, M.; Kimura, E. *J. Chem. Soc., Dalton Trans.* **1977**, 1473.

0020-1669/84/1323-2793$01.50/0